Article

Structure

Crystal Structure of the Peroxo-diiron(III) Intermediate of Deoxyhypusine Hydroxylase, an Oxygenase Involved in Hypusination

Graphical Abstract

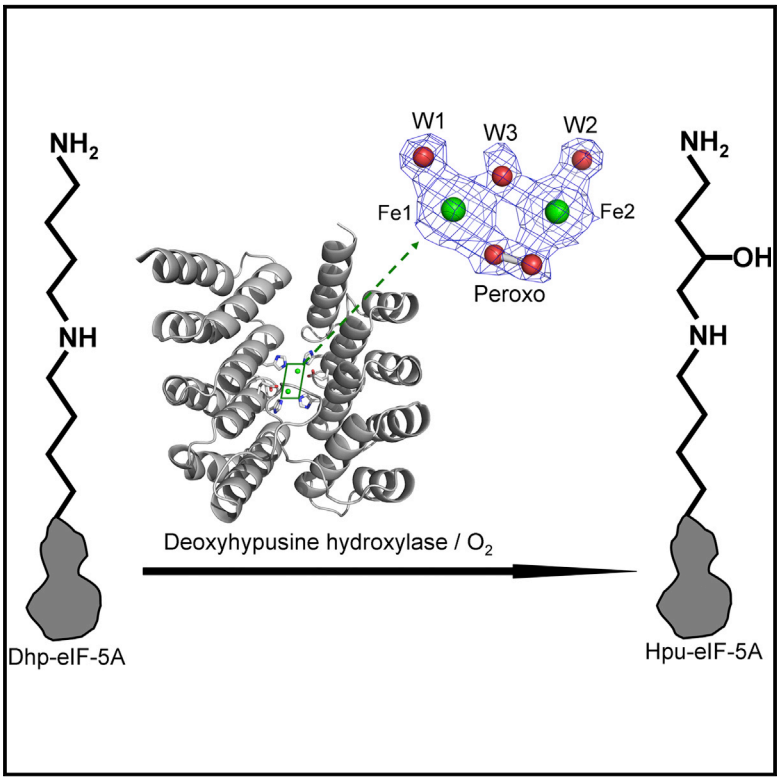

Authors

Zhenggang Han, Naoki Sakai, ..., Alfred X. Trautwein, Rolf Hilgenfeld

Correspondence

hilgenfeld@biochem.uni-luebeck.de

In Brief

Han et al. describe the crystal structure of hDOHH, which catalyzes the second step of hypusination. For the first time, the structure of a native biological diiron(III) peroxo intermediate is revealed at atomic resolution. The structure also shows how hDOHH recognizes its only substrate, deoxyhypusine-eIF-5A.

Highlights

- Spectroscopic studies demonstrate extreme longevity of hDOHH peroxo intermediate
- Crystal structures of hDOHH were solved in two forms, peroxo and glycerol complex
- The diiron core environment explains the unusual stability of the peroxo intermediate
- A docking experiment provides a plausible model for deoxyhypusine binding to hDOHH

Accession Numbers

4D50
4D4Z

Han et al., 2015, Structure *23*, 882–892
May 5, 2015
http://dx.doi.org/10.1016/j.str.2015.03.002

CellPress

Structure
Article

Crystal Structure of the Peroxo-diiron(III) Intermediate of Deoxyhypusine Hydroxylase, an Oxygenase Involved in Hypusination

Zhenggang Han,[1] Naoki Sakai,[1,6] Lars H. Böttger,[2] Sebastián Klinke,[1,7] Joachim Hauber,[3,4] Alfred X. Trautwein,[2] and Rolf Hilgenfeld[1,5,*]

[1]Institute of Biochemistry, Center for Structural and Cell Biology in Medicine, University of Lübeck, Ratzeburger Allee 160, 23538 Lübeck, Germany

[2]Institute of Physics, Center for Structural and Cell Biology in Medicine, University of Lübeck, Ratzeburger Allee 160, 23538 Lübeck, Germany

[3]Heinrich Pette Institute – Leibniz Institute for Experimental Virology, Martinistraße 52, 20251 Hamburg, Germany

[4]German Center for Infection Research (DZIF) c/o Heinrich-Pette-Institute - Leibniz Institute for Experimental Virology, Martinistraße 52, 20251 Hamburg, Germany

[5]German Center for Infection Research (DZIF) c/o Institute of Biochemistry, University of Lübeck, Ratzeburger Allee 160, 23538 Lübeck, Germany

[6]Present address: Structural Biology Group, Division of Structural and Synthetic Biology, RIKEN Center for Life Science Technologies (CLST), 1-7-22 Suehiro-cho, Tsurumi-ku, 230-0045 Yokohama, Japan

[7]Present address: Fundación Instituto Leloir, IIBBA-CONICET, Avenida Patricias Argentinas 435, C1405BWE Buenos Aires, Argentina

*Correspondence: hilgenfeld@biochem.uni-luebeck.de

http://dx.doi.org/10.1016/j.str.2015.03.002

SUMMARY

Deoxyhypusine hydroxylase (DOHH) is a non-heme diiron enzyme involved in the posttranslational modification of a critical lysine residue of eukaryotic translation initiation factor 5A (eIF-5A) to yield the unusual amino acid residue hypusine. This modification is essential for the role of eIF-5A in translation and in nuclear export of a group of specific mRNAs. The diiron center of human DOHH (hDOHH) forms a peroxo-diiron(III) intermediate ($hDOHH_{peroxo}$) when its reduced form reacts with O_2. $hDOHH_{peroxo}$ has a lifetime exceeding that of the peroxo intermediates of other diiron enzymes by several orders of magnitude. Here we report the 1.7-Å crystal structures of $hDOHH_{peroxo}$ and a complex with glycerol. The structure of $hDOHH_{peroxo}$ reveals the presence of a μ-1,2-peroxo-diiron(III) species at the active site. Augmented by UV/Vis and Mössbauer spectroscopic studies, the crystal structures offer explanations for the extreme longevity of $hDOHH_{peroxo}$ and illustrate how the enzyme specifically recognizes its only substrate, deoxyhypusine-eIF-5A.

INTRODUCTION

Translation initiation factor 5A (eIF-5A) is a ubiquitous protein of monomeric molecular mass of around 18 kDa. It is present in archaea and eukaryotes but not in prokaryotes (Park, 2006). A highly conserved lysine residue located in an exposed position in the N-terminal domain of eIF-5A undergoes a unique post-translational modification, hypusination. Hypusination of eIF-5A is achieved in a two-step process involving the enzymes deoxyhypusine synthase (DHS) and deoxyhypusine hydroxylase (DOHH), resulting in extension of the critical lysine residue by a 1-amino-3-hydroxobutyl moiety to become hypusine (Hpu) (Park, 2006) (Figure 1).

eIF-5A is the only protein known to be subject to hypusination (Greganova et al., 2011); this modification is essential for the biological roles of the protein in translation elongation (Saini et al., 2009), in particular of polyproline stretches (Gutierrez et al., 2013). Hypusination of eIF-5A is also essential for nucleocytoplasmic mRNA transport of transcripts encoding inducible nitric oxide synthase and of retroviral mRNA, which are related to islet β-cell dysfunction (Maier et al., 2010) and retroviral replication (Hauber et al., 2005), respectively. Furthermore, the degree of eIF-5A hypusination seems to be relevant for controlling the balance between cell proliferation and apoptosis (Tome and Gerner, 1997; Caraglia et al., 2001, 2013). Prevention of eIF-5A hypusination through inactivating DHS or DOHH is therefore of interest for the development of therapies for the treatment of HIV/AIDS, chronic myeloid leukemia, and diabetes (Kaiser, 2012).

The structure and mechanism of DHS have been extensively characterized (see Park, 2006, for a review). However, progress in research on DOHH remains limited. The atomic structure of DOHH has not been determined although a low-resolution structural model derived from small-angle X-ray scattering has been reported for the yeast enzyme (Cano et al., 2010). Circular dichroism spectroscopy and amino acid sequence analysis revealed that DOHH is an α-helix-rich protein belonging to the HEAT-repeat protein family (Park et al., 2006; Kim et al., 2006; Cano et al., 2010). Molecular modeling and site-directed mutagenesis suggested that human DOHH (hDOHH) is a non-heme diiron enzyme featuring highly conserved His-Glu motifs that offer two potential iron coordination sites (Park et al., 2006; Kim et al., 2006). Recombinant hDOHH is a mixture of apo- and holo-enzyme, which displays two close peaks in gel filtration and different mobilities in native gel electrophoresis (Kim et al., 2006). A considerable proportion of recombinant hDOHH is

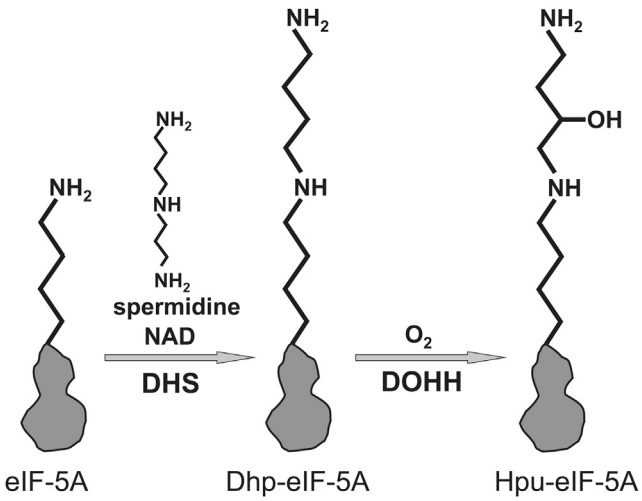

Figure 1. Posttranslational Modification of eIF-5A

Hypusination is a two-step process performed by deoxyhypusine synthase (DHS) and deoxyhypusine hydroxylase (DOHH). The eIF-5A precursor is successively converted to deoxyhypusine-eIF-5A (Dhp-eIF-5A) and hypusine-eIF-5A (Hpu-eIF-5A).

apo-enzyme, which in turn exists as a mixture of several conformations as concluded from a diffuse band in native electrophoresis (Kim et al., 2006).

Recombinant hDOHH is bluish and contains two antiferromagnetically coupled, high-spin Fe(III) atoms, as revealed by Mössbauer spectroscopy (Vu et al., 2009). The characteristic chromophore (two absorption bands at λ_{max} ~320 nm and λ_{max} ~630 nm) is ascribed to the charge transfer between Fe(III) and the O_2^{2-} ligand, suggesting that bluish hDOHH is a peroxo intermediate ($hDOHH_{peroxo}$) (Vu et al., 2009). Charge-transfer bands (630–725 nm) and Mössbauer parameters similar to those of $hDOHH_{peroxo}$ have been found for the peroxo intermediates of soluble methane monooxygenase hydroxylase (sMMOH) (Liu et al., 1995), ribonucleotide reductase subunit R2 (RNR-R2) variants (Moënne-Loccoz et al., 1998), stearoyl-acyl carrier protein Δ^9-desaturase (Δ^9D) (Broadwater et al., 1998), ferritin (Moënne-Loccoz et al., 1999), and the T201S variant of toluene/*o*-xylene monooxygenase hydroxylase (ToMOH) ($T201S_{peroxo}$) (Song et al., 2009; Song and Lippard, 2011). The peroxo-diiron(III) intermediates in these enzymes have been assigned as end-on, bridging peroxo-diiron(III) species (μ-1,2-peroxo-diiron(III)) based on the structures of biomimetic synthetic complexes displaying similar charge-transfer bands, Mössbauer parameters, and Raman bands (Kim and Lippard, 1996; Ookubo et al., 1996; Zhang et al., 2005). In addition to these peroxo-diiron(III) species, it has also been proposed that the peroxo intermediate is present in the reaction cycle of wild-type ToMOH (Murray et al., 2007), *p*-aminobenzoate *N*-oxygenase (AurF) (Korboukh et al., 2009), and aldehyde-deformylating oxygenase (ADO) (Pandelia et al., 2013). However, the peroxo intermediates in these enzymes lack optical bands similar to those of peroxo intermediate of sMMOH implying that the binding mode of the peroxo unit in the diiron(III) core of these enzymes is different from that in ferritin or sMMOH; it likely features a μ-1,1-peroxo geometry (Korboukh et al., 2009). Although it is not an enzyme, oxyhemerythrin (oxyHr) also contains a peroxo-diiron(III) species; however, it has been found that in this case, a non-bridging hydroperoxo ligand terminally binds to only one iron of the diiron site (Klotz and Kurtz, 1984; Holmes et al., 1991).

The peroxo-diiron(III) species detected in all non-heme diiron(III) enzymes exist as transient intermediates with very short lifetimes. Therefore, characterization of the peroxo-diiron(III) species by crystallography is a challenge. After soaking crystals in H_2O_2 (a non-biological peroxide-shunt reaction), Bailey and Fox (2009) reported the structure of a peroxo intermediate of toluene 4-monooxygenase hydroxylase (T4moH) (in complex with effector protein). This structure may not represent the native state of the dioxygen-bound diiron core during O_2-activation, since the peroxo ligand was initially protonated, leading to differences in the proton balance within the active site (Bailey and Fox, 2009). Unusually, $hDOHH_{peroxo}$ displays extreme longevity, as it survives several days after protein purification, even at room temperature (Vu et al., 2009). Therefore, hDOHH is an excellent system to structurally investigate the native biological peroxo-diiron(III) intermediate, thereby providing key information on the mechanisms of O_2-activating non-heme diiron enzymes. An atomic structure is essential to understand the structural properties of the transient intermediate as well as the interaction between hDOHH and its specific substrate, deoxyhypusine-eIF-5A (Dhp-eIF-5A).

In the study presented here, we crystallized hDOHH and determined its three-dimensional structure. We present two crystal structures that correspond to two states of the enzyme, $hDOHH_{peroxo}$ (POX) and a complex of the diiron core with glycerol (GLC). Both structures have a resolution of 1.7 Å. For the first time, the POX structure reveals the atomic details of a native biological μ-1,2-peroxo-diiron(III) intermediate. A unique diiron coordination and the secondary coordination environment explain the extreme longevity of $hDOHH_{peroxo}$. The structure of the glycerol complex serves as a reference for the diiron(III) geometry in the resting state, which is useful for comparison with the peroxo intermediate of the enzyme. The structures also illustrate the properties of the substrate-binding pocket. A model for the hDOHH-Dhp interaction is built on the basis of a docking experiment.

RESULTS AND DISCUSSION

Holo-Enzyme Isolation and Crystallization

Stepwise truncation of the presumably unstructured C-terminal region of hDOHH (total number of residues, 302) was applied in order to increase the chance of crystallizing the enzyme. Truncated hDOHH was overproduced in *Escherichia coli* as described in the Experimental Procedures. The pure holoenzyme was isolated by repeated gel filtration until the apo-hDOHH was almost completely removed from isolated hDOHH (Figure S1A). A construct truncated at Gln289 gave rise to the best crystallization hit. Crystals were obtained within ~6 hr of setting up the crystallization experiment and were of weak blue color (Figure S1B). When 10%–20% glycerol was applied as a crystallization additive, the crystals grew much more slowly, within ~36 hr, and were mostly colorless to light brownish (Figure S1C).

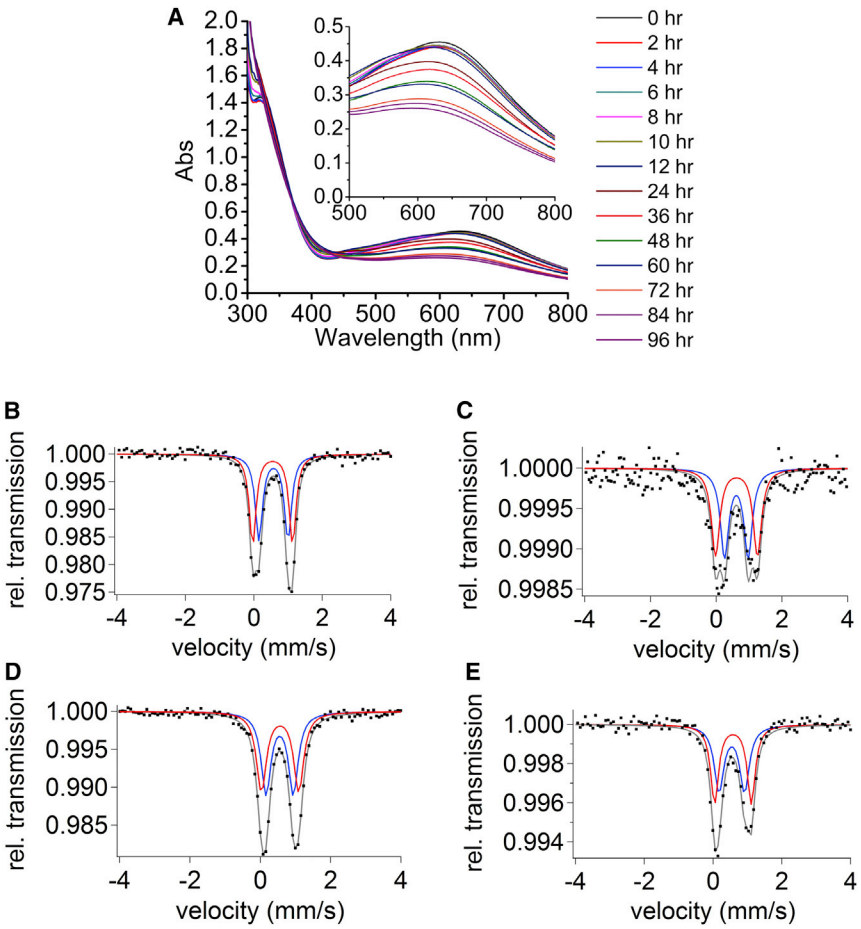

Figure 2. Spectroscopic Results

(A) Time-dependent UV/Vis absorption spectra recorded at 10°C. The inset shows a magnification of the absorption peak at long wavelengths.

(B) Mössbauer spectrum of freshly isolated hDOHH in solution.

(C) Mössbauer spectrum of hDOHH polycrystals grown for 48 hr. The crystallization conditions were the same as for crystals used for X-ray diffraction (see Figure S1B).

(D) Mössbauer spectrum of hDOHH in solution in the presence of 10% glycerol, 48 hr after isolation.

(E) Mössbauer spectrum of polycrystals of the hDOHH-glycerol complex grown for 48 hr. The crystallization conditions were the same as for glycerol-containing crystals used for X-ray diffraction (see Figure S1C).

Spectroscopic Studies

The characteristic bluish color of hDOHH (Vu et al., 2009) showed up immediately after breaking the expression cells. The color persisted during the process of protein purification at 4°C. Even if the protein purification time for individual batches varied from 2 to 5 days, the same profiles in the UV/Vis spectra were observed. Time-dependent UV/Vis spectra recorded at 10°C (the temperature of crystallization; see below) revealed that the absorption band at long wavelengths was blue-shifted from λ_{max} ~630 nm to λ_{max} ~ 600 nm within ~96 hr, concomitant with a reduction of molar absorptivity (Figure 2A); at room temperature, this effect was somewhat stronger (data not shown). The lack of pure isosbestic points in the spectra suggests the presence of more than one decay species of the initial peroxo intermediate during the recorded period. The persisting, albeit weaker, blue color of this hDOHH solution indicates the continued presence of peroxo-diiron(III) species. Similar blue-shifts of the maximum absorbance coupled with reduced molar absorptivity have been ascribed to changes in the protonation state or to a carboxylate shift in the peroxo-diiron(III) core, for instance in ferritin (Bou-Abdallah et al., 2005) or in synthetic model compounds (Zhang et al., 2005; Frisch et al., 2009). From an inspection of the UV/Vis spectra, we therefore assume that, due to a similar process, more than one peroxo-diiron(III) species is present in the hDOHH system.

In order to characterize possible changes at the diiron site in the crystalline state, polycrystals were prepared of the free enzyme as isolated and of the glycerol-containing sample, and subjected to Mössbauer spectroscopy. Freshly isolated hDOHH in solution was measured in parallel as a reference. The latter gave Mössbauer parameters $\delta_{1/2}$ = 0.57/0.55 mm s^{-1}, $\Delta E_{Q1/2}$ = 0.85/1.17 mm s^{-1}, $\Gamma_{1/2}$ = 0.27/0.24 mm s^{-1} (Figure 2B), almost identical to the results reported by Vu et al. (2009). This spectrum shows very narrow line widths, suggesting that our purified hDOHH sample contains a relatively homogenous $hDOHH_{peroxo}$. Crystals of the recombinant enzyme as isolated gave rise to a Mössbauer spectrum slightly different from that obtained from freshly prepared hDOHH in solution (Figure 2C): isomer shifts ($\delta_{1/2}$ = 0.62/0.62 mm s^{-1}, $\Delta E_{Q1/2}$ = 0.72/1.25 mm s^{-1}) were slightly larger than those from freshly prepared hDOHH in solution but still well within the region typical for μ-1,2-peroxo-diiron(III) species (Friedle et al., 2010). The procedure of growing crystals within a given time window (48 hr) and subsequent washing of the crystals with buffer (see Experimental Procedures) set limits to the measured signal-to-noise effect (ca. 0.3%). The crystals grown in the presence of glycerol gave Mössbauer parameters almost identical to a sample of the enzyme in solution containing 10% glycerol (Figures 2D and 2E): $\delta_{1/2}$ = 0.54/0.58 mm s^{-1}, $\Delta E_{Q1/2}$ = 0.74/1.07 mm s^{-1}, $\Gamma_{1/2}$ = 0.33/0.28 mm s^{-1} and $\delta_{1/2}$ = 0.55/0.56 mm s^{-1}, $\Delta E_{1/2}$ = 0.77/1.06 mm s^{-1}, $\Gamma_{1/2}$ = 0.33/0.34 mm s^{-1} for crystals and solution, respectively, which are, however, different from preparations of the free enzyme. The spectra shown in Figures 2D and 2E imply that glycerol likely induces some change at the diiron site of hDOHH. Interestingly, glycerol has been found to accelerate decay of the peroxo-diiron(III) species in sMMOH but the reason is unclear (Lee and Lipscomb, 1999).

Crystal Structure Determination and Overall Structure of hDOHH

For both crystallization conditions, the crystals obtained were harvested after 48 hr (at 10°C) for X-ray diffraction experiments;

Table 1. Crystallographic Data and Refinement Statistics

	Crystal 1 (GLC) (Peak)	Crystal 2 (GLC)	Crystal 3 (POX)
Diffraction Data Statistics			
X-Ray source	BL14.2, BESSY II	BL14.2, BESSY II	BL14.2, BESSY II
Wavelength (Å)	1.73965	0.91841	0.91841
Space group	$P2_1$	$P2_1$	$P2_1$
Unit cell parameters			
a, *b*, *c* (Å)	45.97, 70.22, 101.00	46.05, 70.18, 101.28	45.93, 48.64, 124.09
β (degrees)	102.57	102.71	99.27
Resolution (range) (Å)[a]	27.6–1.90 (2.00–1.90)	44.92–1.70 (1.79–1.70)	19.85–1.70 (1.79–1.70)
Reflections	328,812 (44,594)	269,456 (26,602)	193,329 (30,445)
Unique reflections	49,878 (7,266)	68,054 (8,949)	57,441 (8,631)
R_{merge}	0.075 (0.260)	0.037 (0.174)	0.049 (0.237)
R_{pim}[b]	0.031 (0.116)	0.021 (0.121)	0.032 (0.148)
$CC_{1/2}$	0.997 (0.894)	0.999 (0.962)	0.998 (0.938)
$I/\sigma(I)$	17.1 (6.9)	23.5 (6.0)	14.0 (4.3)
Redundancy	6.6 (6.1)	4.0 (3.0)	3.4 (3.5)
Completeness (%)	99.8 (99.8)	98.2 (89.0)	96.2 (99.7)
Wilson B factor (Å^2)	20.6	17.2	14.9
SigAno	2.00		
FOM (DM FOM)	0.694 (0.855)		
Refinement Statistics[c]			
Refinement resolution range (Å)		19.95–1.70	19.85–1.70
No. of reflections		64,571	54,485
R_{work}/R_{free} (% of reflections)		0.171/0.194 (5.0)	0.203/0.246 (5.0)
Average B factor (Å^2)		20.67	18.90
No. of atoms			
Protein		4399	4410
Water		335	440
Other		37	28
Rms deviations			
Bond lengths (Å)		0.022	0.018
Bond angles (degrees)		2.007	1.769
Ramachandran favored (%)		100.00	99.30
Ramachandran outliers (%)		0.00	0.00
MolProbity score		1.58	1.78

[a]The highest resolution shell is shown in parentheses.
[b]Precision-indicating merging *R* factor. R_{pim} is defined as $\Sigma_{hkl}[1/(N-1)]^{1/2} \Sigma_i|I_i(hkl) - \langle I(hkl)\rangle|/\Sigma_{hkl}\Sigma_i^{I_i(hkl)}$ (Weiss and Hilgenfeld, 1997).
[c]See also Table S1.

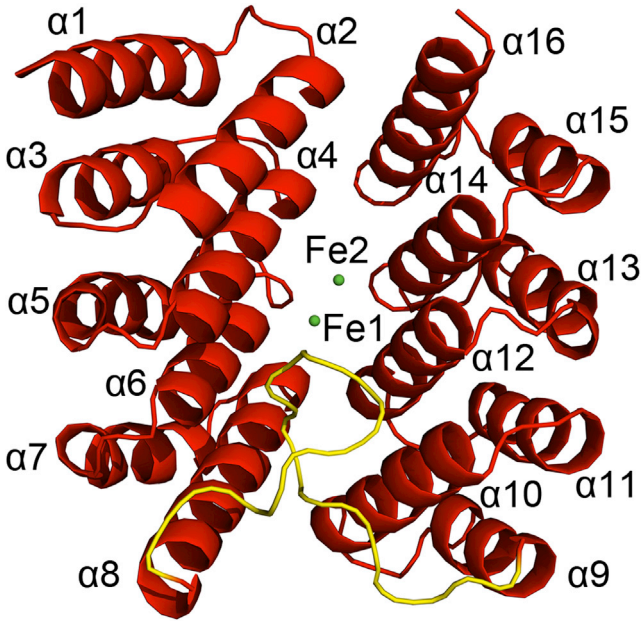

Figure 3. Ribbon Presentation of the Structure of hDOHH
Helices are labeled. Yellow, inter-domain loop; green, iron atoms. See also Figures S2 and S3.

thus, the structures obtained likely correspond to enzyme subjected to similar aging conditions as the samples used for Mössbauer (crystalline preparations) and UV/Vis (48 hr) spectroscopy.

The crystals grown from the glycerol-free and glycerol-containing conditions share the same space group but display different unit cell parameters. The refined structures feature two different states of the diiron core, the peroxo-diiron(III) intermediate (POX) in the crystals grown in the absence of glycerol and a glycerol-bound diiron complex (GLC) in the crystals grown in the presence of glycerol. Both structures have a resolution of 1.7 Å. Table 1 shows a summary of diffraction data collection, phase determination, and structure refinement.

Both structures (POX and GLC) have an almost identical overall architecture. There are two hDOHH monomers (A and B) per asymmetric unit. The overall structure of the hDOHH monomer comprises a pseudosymmetric arrangement of an N-terminal and a C-terminal domain, each consisting of four HEAT repeats (α-hairpins), accounting for a total of 16 α-helices, as predicted by sequence analysis (Park et al., 2006) (Figure 3). There is no related structure in the PDB with 4 + 4 HEAT repeats. In each of the two domains, the four HEAT motifs stack on top of each other, with odd-numbered α-helices (α1, 3, 5, 7, and 9, 11, 13, 15) arranged parallel to one another and located toward the exterior of the protein, and even-numbered α-helices (α2, 4, 6, 8, and 10, 12, 14, 16) also arranged parallel to one another and located in the interior of the protein (Figure 3). The interior α-helix layers from the two domains pack against each other at an angle of approximately 45°, leaving an opening that runs along the interface in the middle of the protein. A significant deviation between the POX and GLC structures exists at the C-terminal helices, in particular α16 (Figure S2). The reorientation of α16 by an angle of around 15° results in a difference of 6.07 ± 0.15 Å for the

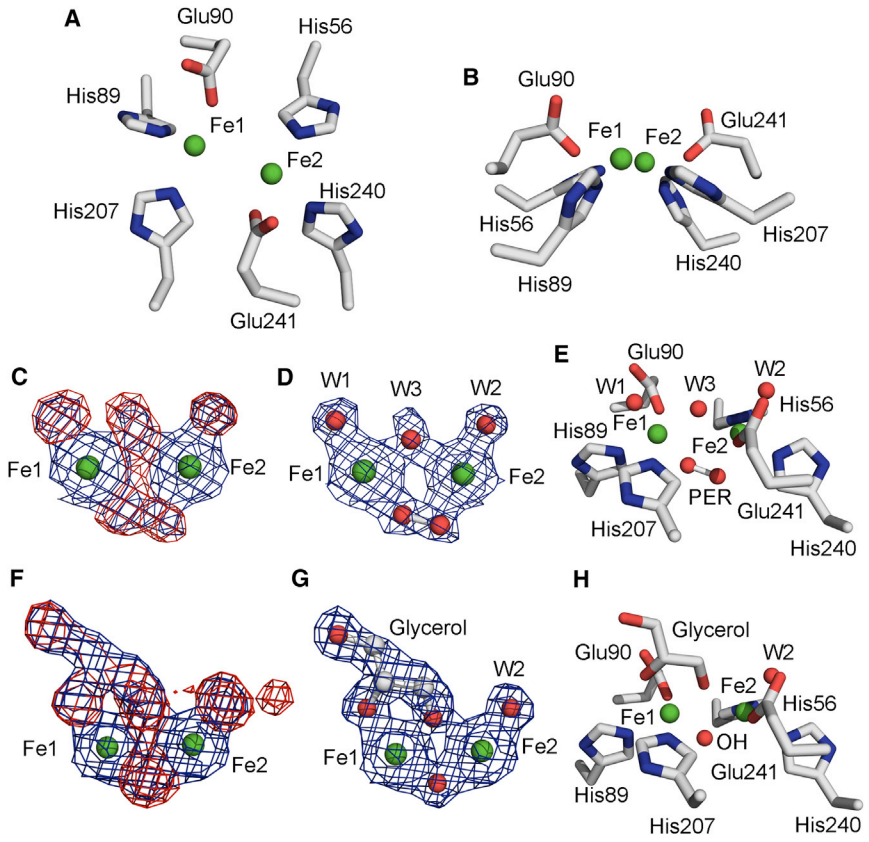

Figure 4. Electron Density Maps and Coordination Geometry of the Diiron Core

Carbon, nitrogen, oxygen, and iron atoms are presented in gray, blue, red, and green, respectively. PER, peroxide ion; W1, water coordinating to Fe1; W2, water coordinating to Fe2; W3, bridging water. The electron density maps for molecule B are presented in Figure S4.

(A) Amino acid residues as diiron core ligands in hDOHH.

(B) As in (A), in another orientation (180° counterclockwise rotation of (A), viewed from the side of His89 and His207).

(C) Electron density around the iron atoms in chain A of the POX structure before including the non-protein ligands: magenta, $F_o - F_c$ map (contoured at 4.0σ); blue, $2F_o - F_c$ map (at 1.0σ).

(D) Electron density map of the diiron core in chain A of the POX structure after ligand inclusion and refinement ($2F_o - F_c$ map, at 1.5σ, blue mesh).

(E) The diiron core in chain A of the POX structure with the non-protein ligands included.

(F) As in (C), for the GLC structure.

(G) As in (D), for the GLC structure.

(H) As in (E), for the GLC structure.

C-terminal residue, Glu283, of this helix (for the Cα position; averaged between the two copies in the asymmetric unit).

The N-terminal and the C-terminal domains share 36% sequence identity (53% similarity) (Figure S3) and the structures of the two domains can be superimposed with a Cα root-mean-square (rms) difference of about 0.95 Å, strongly suggesting that hDOHH evolved through gene duplication. The two domains are connected by a long loop (residues 136–157), the conformation of which is very well conserved between the four copies of hDOHH (POX and GLC) elucidated within this study (Figure 3). The loop invaginates into the interior of the protein where it is involved in several electrostatic interactions. Between the two domains, near the helix pairs α4/α6 and α12/α14, the diiron catalytic center of hDOHH is located in an orientation parallel to the axis between the two staples of HEAT repeats (Figure 3).

Diiron Core of hDOHH

The diiron centers of the POX and GLC structures share the same set of amino acid ligands. Each iron is coordinated by two histidine residues (through their Nε atoms) and one glutamate; thus, the diiron center of hDOHH displays a histidine-rich coordination, 4H-2E (Figure 4A). Fe1 is coordinated by His89, Glu90, and His207, and Fe2 is coordinated by His56, His240, and Glu241. In previous mutagenesis work, all these residues were found to be essential for maintaining the iron content and activity of the enzyme (Kim et al., 2006). All amino acid ligands of the Fe atoms are monodentate; distinct from other diiron enzymes (Nordlund and Eklund, 1995; Summa et al., 1999), there is no bridging glutamate. The coordinative bonds to the carboxylate oxygens range from 1.99 to 2.10 Å, whereas the Fe-N bonds are between 2.18 and 2.34 Å. All four histidines coordinate to the same hemisphere of the diiron core and the four Nε atoms from the histidines are approximately arranged in one plane (Figure 4B).

In the POX structure, the distance between the two Fe atoms is 3.77 and 3.68 Å in the two copies of the enzyme. In a cavity within the histidine coordination hemisphere, we detected a well-defined difference density that could be clearly assigned to a peroxo ligand in an orientation roughly but not exactly parallel to the Fe-Fe axis (Figures 4C and 4D; Figures S4A and S4B). This presumed O_2^{2-} species bridges the irons as a μ-1,2-ligand at distances of 2.23/2.21 Å (Fe1) and 2.18/2.17 Å (Fe2) (Figure 4E; Table S1). The O-O bond length is 1.54/1.52 Å (for molecules A and B, respectively), and the B factors for the individual oxygens are almost equal to one another (Table S1). The Fe-O-O-Fe torsion angles are −58.1 and −31.6° (gauche conformation) in molecules A and B, respectively. In addition, on the opposite side of the Fe-Fe axis, in the upper coordination hemisphere of the diiron core, there are three water molecules (W1, W2, and W3) coordinating to diiron, with W3 bridging the two irons (Figures 4D and 4E). W3 could also be a bridging hydroxo ion as proposed by Vu et al. (2009) on the basis of spectroscopic studies and structures of model complexes.

The Fe-Fe distances of 3.77/3.68 Å are within the range observed in structures of biomimetic complexes, where the distances vary from 3.17 to 4.00 Å (Kim and Lippard, 1996; Dong et al., 1996; Ookubo et al., 1996; Zhang et al., 2005). The value of ~3.7 Å for the POX structure is slightly longer than the 3.44 Å Fe-Fe distance determined for $hDOHH_{peroxo}$ by extended X-ray absorption fine structure spectroscopy

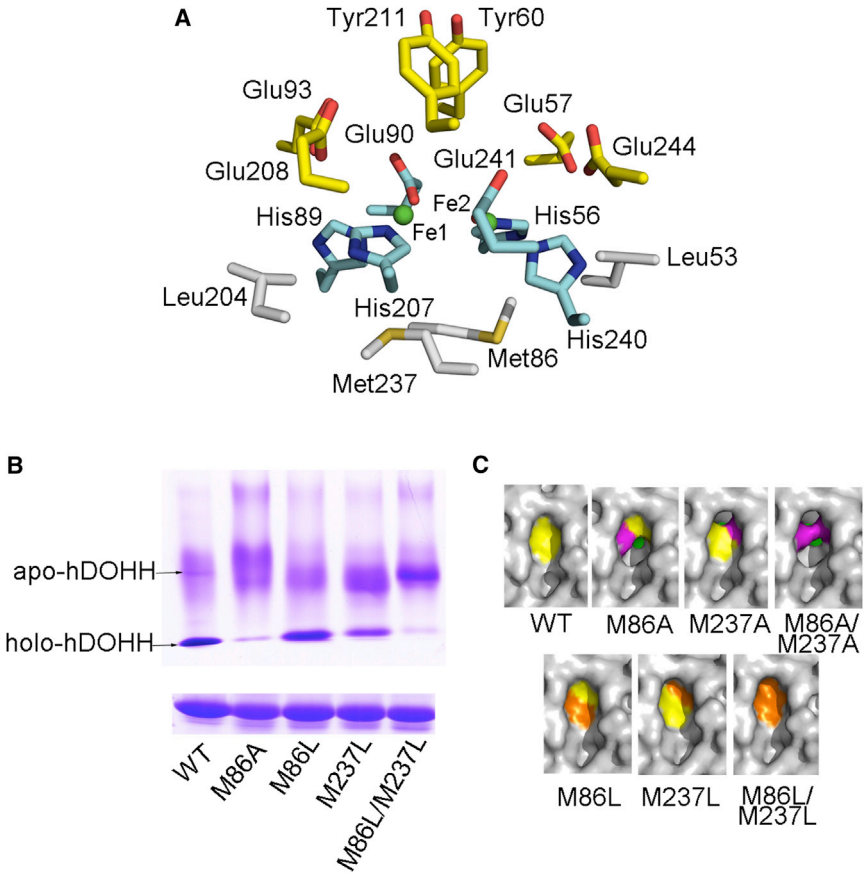

Figure 5. Residues in the Secondary Coordination Sphere of the Diiron Core of hDOHH

(A) The diiron core in hDOHH with the secondary coordination sphere included. The carbon atoms of residues in the primary coordination sphere are cyan, those of residues in the hydrophobic secondary hemisphere (below the Fe-Fe axis) are gray, and those in the hydrophilic secondary hemisphere (above the Fe-Fe axis) are yellow.

(B) Methionine mutations at positions 86 and 237: SDS-PAGE (bottom) and native PAGE (top).

(C) The methionine pair Met86/Met237 shields the diiron core from solvent. Both methionines have been replaced either separately or together by alanine or leucine in site-directed mutagenesis experiments (see text and (B)). The figure shows a model of the modified residues based on the crystal structure (POX) of wild-type hDOHH. In the wild-type structure (yellow surfaces for Met86 and Met237) and the leucine mutants (orange surfaces), the iron atoms (green spheres) are shielded by a pair of large hydrophobic residues (and consequently not visible in these images), but in the alanine mutants (magenta surfaces), the iron is accessible to solvent.

(Vu et al., 2009). The elongated Fe-Fe distance in our crystal structure is possibly due to aging during the process of crystallization (at 10°C over 48 hr) that might be accompanied by protonation of a bridging hydroxyl ion to water (W3) in the diiron core of POX, which would result in a longer Fe-Fe distance. Ranging between 2.17 and 2.23 Å, the Fe-O(peroxo) distances are longer than the values of 1.86–1.94 Å observed in biomimetic model complexes (Kim and Lippard, 1996; Ookubo et al., 1996; Zhang et al., 2005). The elongated Fe-O(peroxo) distances in the POX structure could result from protonation of the bridging peroxo unit, as proposed for large Fe-O(peroxo) distances in the structure of the non-biological T4moH peroxo intermediate obtained by soaking crystals with H_2O_2 (Bailey and Fox, 2009).

In the GLC structure, the Fe-Fe distance has shrunk to 3.44/3.48 Å. There is no electron density consistent with the presence of a peroxo ligand; both F_o - F_c and $2F_o$ - F_c maps reveal a single oxygen atom as a bridging ligand in the lower hemisphere and a glycerol molecule bound to the upper hemisphere of the diiron core (Figures 4F and 4G; Figures S4C and S4D). In the refined GLC structure, the distances between Fe and the bridging oxygen are 2.05/1.95 Å (Fe1) and 2.21/2.22 Å (Fe2) (Table S1). Fe-O-Fe angles are 107.5 and 113.2° in the two molecules of the GLC structure, consistent with the bridging oxygen being a μ-hydroxo ligand (Kurtz, 1990). In the other ligation hemisphere, hydroxyl group 2 (O2) of glycerol replaces W1 of the POX structure and hydroxyl group 3 (O3) replaces the bridging W3 (Figure 4H). Hydroxyl group 1 (O1) of glycerol donates a bifurcated hydrogen bond to the carboxylates of Glu93 and Glu208. A glycerol-bound diiron site is also present in the X-ray structure of phenol hydroxylase (PH), but in a different binding mode, with the O2 of glycerol coordinating to Fe1 only and the other two hydroxyl groups not being involved in iron coordination (McCormick and Lippard, 2011).

Secondary Coordination Sphere of the Diiron Site in hDOHH

Surrounding the 4H-2E set of ligands, a number of amino acid side chains constitute a secondary coordination sphere for the diiron cluster in hDOHH. Like the iron ligands of the inner sphere, all residues in the secondary coordination sphere are present in pairs (one mate from each of the two domains) and arranged symmetrically around the diiron center (Figure 5A). The secondary coordination sphere can be divided into a hydrophilic hemisphere above the Fe-Fe axis and a hydrophobic hemisphere below the Fe-Fe axis (on the peroxo side of the diiron core) in Figure 5A. In the hydrophilic hemisphere, two glutamate pairs (Glu57/Glu244 and Glu93/Glu208) are located at each end of the diiron unit; a hydrogen-bonded tyrosine pair (Tyr60/Tyr211) is around 9 Å (terminal OH group to Fe) above the diiron site. Alanine substitutions of glutamates 57, 93, and 208 do not affect the iron content (Kang et al., 2007); nor does the E244A mutation (Z.H. et al., unpublished data).

In the hydrophobic hemisphere, residue pairs Leu53/Leu204 and Met86/Met237 as well as the four iron-coordinating histidines (His56, His89, His207, and His240) enclose the small pocket containing the peroxo ligand below the diiron unit, with Met86 and Met237 shielding the diiron core from solvent (Figure 5A). The methionine pair is absolutely conserved in DOHH.

It displays 180° rotational symmetry and is located ~5.5 Å (Fe-S(Met) distance) away from the diiron unit (Figure 5A). The electron density maps suggest that there are alternative conformations for the tips of the side chains of Met86 and Met237.

Although Met237 and Met86 are not coordinating the iron atoms directly, they influence the proper function of hDOHH. The M237A mutation has been reported to lead to loss of iron and enzymatic activity (Kang et al., 2007). In separate experiments, we replaced Met86 by alanine and one or both of the methionines by leucine. The mutations M86A and M86L/M237L lead to serious loss of iron, whereas M237L leads to partial loss of the metal ions (Figure 5B). Structural modeling of the methionine mutations shows that the alanine substitutions make the diiron core solvent accessible but the leucine mutants do not (Figure 5C). Yet, the presence of at least one methionine is required to retain hDOHH in the holo-enzyme state. A possible role for the methionine pair might be protection of the diiron core by scavenging reactive oxygen species.

Structural Basis for the Extreme Longevity of the Peroxo-diiron(III) Intermediate in hDOHH

Generally, the fate of peroxo-diiron(III) species in O_2-activating non-heme diiron enzymes is cleavage of the O-O bond and concomitant oxidation of the diiron core to high-oxidation-state diiron species, which are the ones performing the respective catalytic reactions (Wallar and Lipscomb, 1996). The lifetime of the peroxo-diiron(III) core in enzymes of this kind is very short (half-life varies from seconds to 30 min) (Table S2). In contrast, $hDOHH_{peroxo}$ is unusually stable (Figure 2A; Table S2). A structural comparison of the diiron environment of other peroxo-diiron(III) enzymes with hDOHH sheds light on the reasons for the extreme longevity of $hDOHH_{peroxo}$. First, a histidine-rich ligand set (4H-2E) coordinates the diiron unit; all histidines coordinate iron through their Nε atoms; both glutamate carboxylate groups are terminal ligands for the iron atoms in a monodentate fashion. All of these features weaken the electron-donating properties of the iron ligands. Studies with biomimetic complexes revealed that cleavage of the O-O bond is enhanced by introduction of more electron-donating, negatively charged ligands (Dong et al., 1996). In contrast to hDOHH, the diiron sites of sMMOH, RNR-R2, and Δ^9D display a carboxylate-rich ligand set, histidines coordinating through their Nδ atoms, and at least one bridging carboxylate (Table S2). Second, the peroxo unit in $hDOHH_{peroxo}$ is shielded by a unique, highly hydrophobic environment (Figure 5A) comprising the four histidines as well as the residue pairs Met86/Met237 and Leu53/Leu204. A correlation between the stability of the peroxo species and the hydrophobicity of its environment has been observed with small-molecule model compounds. A μ-1,2-peroxo-diiron(III) model complex, in which the peroxo ligands are located in a hydrophobic pocket consisting of phenyl groups, shows significant thermal stability and reversible oxygenation (Ookubo et al., 1996). In addition, such a hydrophobic environment for the peroxo unit avoids proton-triggered heterolytic O-O bond cleavage. A threonine residue in the vicinity of the diiron sites of sMMOH, ToMOH, and Δ^9D may play a role in O_2 binding and transferring protons to the peroxo unit (Wallar and Lipscomb, 1996; Bochevarov et al., 2011; Lee et al., 2013). It has been shown that this threonine accelerates the formation and decay rates of the peroxo intermediates of ToMOH (Song et al., 2010). The presumably corresponding position in hDOHH is occupied by the methionine pair, Met86/Met237, which is not a good candidate for mediating proton transfer.

On the basis of these observations, we propose that the unique diiron environment in hDOHH blocks the oxygen activation sequence at the stage of the peroxo-diiron(III) species. This means that the catalytic core of hDOHH has very limited ability to break the O-O bond and generate a potent oxidant for C-H bond cleavage, in agreement with the observed, extremely low activity of hDOHH in vitro (Vu et al., 2009). The decay of $hDOHH_{peroxo}$ is accelerated in the presence of protein substrate (Vu et al., 2009), implying that incorporation of the Dhp side chain into the diiron site facilitates the electron transfer. Vu et al. (2009) suggested that perhaps a so far unidentified interaction partner exists in vivo that assists the reaction. Alternatively, Nature perhaps chose such a slow enzyme to modulate the hypusination of eIF-5A, by which cell growth is strictly regulated (Hanauske-Abel et al., 1994).

Although the function of hemerythrin (Hr) is distinct from the O_2-activating non-heme diiron enzymes mentioned above, it is a good example for illustrating how a non-heme diiron protein can maintain the integrity of the O-O bond in the peroxo-diiron(III) unit. There are many similarities shared by the peroxo-diiron(III) cores of oxyHr and hDOHH, although the peroxo group binds to the diiron core in different ways. The diiron unit of Hr is coordinated by five histidine ligands (through their Nε atoms) and two carboxylate groups (5H-E-D); the peroxo ion is surrounded by a hydrophobic environment consisting of two leucines, one isoleucine, one phenylalanine, and one tryptophan as well as four iron-coordinating histidines (Stenkamp, 1994), a similar environment to that found in hDOHH (Figure 5A). These characteristics probably allow Hr to function as an O_2 carrier.

The Substrate-Binding Cavity of hDOHH

The mouth of a funnel-shaped access cavity to the active site is located on the surface of hDOHH, on the open side between the two stacks of HEAT repeats. This opening is between 14.5 and 18 Å wide and lined by residues from helix α2 (Gln22, Arg26, Phe29, Arg32), α12 (Gln215, Gln217), and α16 (Asp278, Met279, His282, Glu283) as well as by Leu145 and Ser146 from the inter-domain loop (Figure 6A). About 18 Å into the cavity, a major constriction of the funnel is reached; through the arrangement of amino acid side chains from helices α4 (Glu57, Tyr60), α12 (Tyr211), and α14 (Glu241, Glu244), the diameter is narrowed to 6.5–9.0 Å (Figure 6A). This is the entrance to the inner cavity of the enzyme, which is about 11 Å deep and harbors the diiron active site at one of its walls in an orientation parallel to the long axis of the cavity (Figure 6B). Residues Glu93 and Glu208 are at the bottom of the inner cavity. These properties are in remarkable agreement with an early prediction based on two inhibitory catechol peptide probes anchored to the metal ions through their dihydroxybenzene groups (Abbruzzese et al., 1991).

The dimension of the external cavity is sufficiently wide to accommodate the exposed loop of eIF-5A that carries the Dhp residue to be hydroxylated by hDOHH. The inner cavity is perfectly suited to harbor the Dhp side chain of the substrate and the Hpu product. The electrostatic potential of the

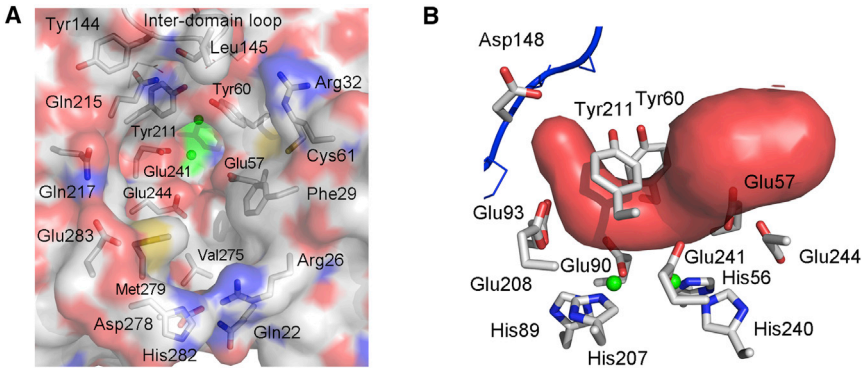

Figure 6. The Substrate-Binding Cavity of hDOHH

(A) View into the substrate funnel, onto the constriction at Tyr60, Tyr211, Glu241, Glu244, and Glu57, which forms the mouth of the inner cavity, the binding site for Dhp and Hpu.

(B) The shape of the cavity and its environment.

(C) Surface electrostatics of hDOHH colored from red (negative potential) to blue (positive potential). The circle indicates the outer rim of the binding site.

(D) As in (C), for human eIF-5A (PDB code 1FH4) (Facchiano et al., 2001). The presumed interacting region of eIF-5A is indicated by the rectangle. Two orientations of the eIF-5A molecule are shown.

substrate-binding site is negative in both the inner and the external cavities (Figure 6C), in agreement with the long, basic side chain of Dhp and the very basic, exposed hydrophilic loop (KTGK$_{50}$HGHAK) of the substrate, Dhp-eIF-5A (Figure 6D).

A Model for Dhp-eIF-5A Binding to hDOHH

In order to build a binding model of Dhp/Hpu in the active center of hDOHH, an automated docking experiment was carried out as part of this study. Dhp and Hpu were docked to hDOHH by using AutoDock (Morris et al., 2009). The results show that the side chain of the Dhp/Hpu residue is neatly accommodated by the inner cavity of hDOHH (Figures 7A and 7B). In the modeled Dhp complex, the terminal ammonium group of Dhp forms strong hydrogen bonds with the Oε2 atoms of Glu93 and Glu208, and its Nε atom hydrogen bonds with Glu241 Oε2 (Figure 7A). Compared with the hDOHH-Dhp (substrate) complex, the structure of the hDOHH-Hpu (product) complex shows some interesting differences. The Hpu moves slightly out from the inner cavity (Figure 7B). The terminal ammonium group of Hpu switches to Glu93 Oε2 and the hydroxyl group of Hpu forms a hydrogen bond with Glu90 Oε2 (Figure 7B). Upon hydroxylation, the modified carbon atom moves from near Fe1 in the hDOHH-Dhp complex to a position in the middle between the two iron atoms, above the diiron site (Figures 7A and 7B). These docking results are in good agreement with the previous observation of an essential role of Glu90, Glu208, and Glu241 for substrate binding (Kang et al., 2007).

Although a large polypeptide (residues 20–90) around the Dhp residue in eIF-5A is needed for an effective enzyme-substrate interaction (Kang et al., 2007), the docking results with Dhp and Hpu alone still provide many hints for understanding the molecular interactions between hDOHH and its only substrate, Dhp-eIF-5A, and they are in agreement with the substrate-binding information obtained from mutagenesis experiments and from our crystal structures. In addition, we observed that the binding mode of glycerol in our GLC structure superimposes perfectly with the terminus of Hpu (terminal three carbons) in the docked structure (Figures 7B and 7C); thus, glycerol can be considered a model for the product of the DOHH reaction.

Conclusions

DOHH is a non-heme diiron enzyme that catalyzes the second and last step of the posttranslational modification of eIF-5A. Mössbauer spectra demonstrated that our recombinant hDOHH preparation contains a relatively homogeneous peroxo-diiron(III) core. This peroxo-diiron(III) intermediate is extremely stable at 4°C, and likely slowly converts to other peroxo-diiron(III) species at higher temperature. By X-ray crystallography of hDOHH$_{peroxo}$, we achieved the first visualization of a native, biological μ-1,2-peroxo-diiron(III) core at atomic resolution, thereby shedding light on the exact geometry of the critical intermediate of O_2-activating non-heme diiron enzymes. At the same time, we elucidated the structural basis for the extreme longevity of the peroxo-diiron(III) intermediate in hDOHH, namely a histidine-rich primary coordination sphere lacking bridging carboxylate ligands, and a hydrophobic secondary coordination hemisphere.

The changes in time-dependent UV/Vis spectra of freshly isolated hDOHH over a period of 48 hr and the slightly different Mössbauer spectrum of hDOHH polycrystals harvested after 48 hr, compared with that of the fresh preparation (Figure 2), indicate that a discrete peroxo species converted from the one initially formed after activation by O_2. The geometry of the peroxo-diiron core observed in the POX structure (derived from a crystal grown in the same time window, 48 hr) displays a relatively loose μ-1,2-peroxo-diiron(III) geometry (large Fe-Fe and Fe-O(peroxo) distances). Very likely, our POX structure represents a putative secondary peroxo-diiron(III) species, which

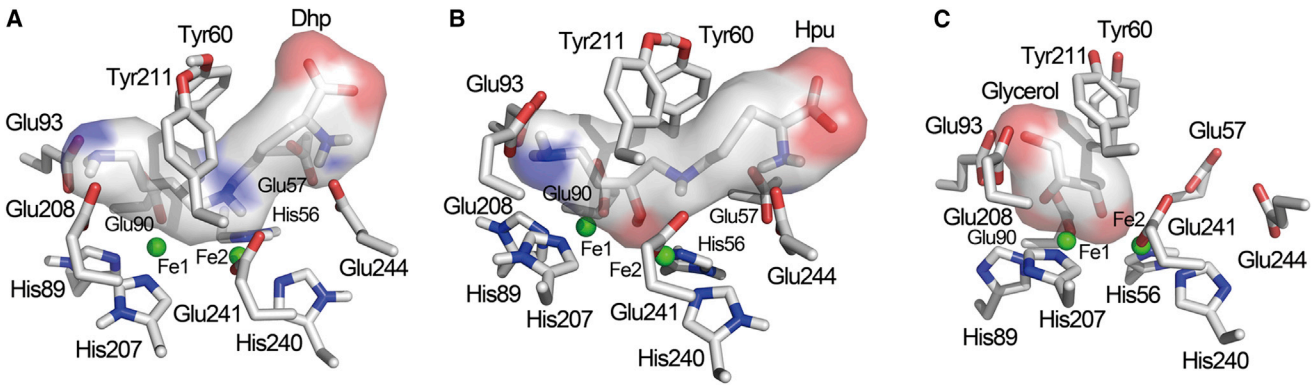

Figure 7. A Model of the hDOHH-Dhp/Hpu Interaction

Carbon, nitrogen, oxygen, and iron atoms are presented in gray, blue, red, and green, respectively. A surface representation of these compounds is also shown.

(A) Docking structure of the hDOHH-Dhp complex.

(B) As in (A), for hDOHH-Hpu.

(C) Glycerol in the substrate cavity in the GLC structure.

corresponds to the enzyme aged within the time window of 48 hr, as characterized by UV/Vis and Mössbauer spectroscopy (Figures 2A and 2C). It is possibly formed by protonation of the non-protein ligands of the diiron site, likely of an oxygen in the peroxo ligand. Such protonation has been proposed as the first step of cleavage of the O-O bond in the well-studied MMOH system (Solomon et al., 2000; Xue et al., 2008). In order to better understand the mechanism of DOHH, more diiron intermediates in the reaction cycle need to be identified.

The electron transfer sequence after the breakdown of $hDOHH_{peroxo}$ remains unclear. It is likely that hDOHH uses a mechanism similar to that of sMMOH, since both these enzymes catalyze the cleavage of a C-H bond and incorporation of a hydroxyl group into the hydrocarbon substrate. Following protonation, the O-O bond is cleaved in sMMOH, yielding a μ-oxo-diiron(IV) core at the active site of the enzyme (compound Q) (Wallar and Lipscomb, 1996). So far, a high-oxidation-state diiron species has not been found for hDOHH. Unusually, the diiron(III) species at the end of the oxidation sequence, which is normally well characterized for other diiron enzymes, has not been observed for the hDOHH system. In our glycerol complex (GLC) structure, the two iron atoms are bridged by a putative hydroxo group, which probably corresponds to the diiron(III) species of hDOHH in the resting state. In addition, a reduction system likely required for hDOHH to regenerate the O_2-reactive state (diiron(II) core) remains to be identified.

The crystal structures of hDOHH help in understanding the specific interaction between hDOHH and Dhp-eIF-5A and provide a basis for the design of inhibitors that could be developed into drugs for the treatment of various diseases. Equally important, they help in understanding the extreme longevity of the peroxo-diiron(III) intermediate in hDOHH and will motivate more spectroscopic studies with this remarkable system.

EXPERIMENTAL PROCEDURES

Expression and Purification

Genes coding for C-terminally truncated hDOHH were cloned into pGEX-6P-1 (GE Healthcare). Site-directed mutagenesis was done using *Pfx* polymerase (Invitrogen). All constructs used for recombinant hDOHH production were confirmed by sequencing. *Escherichia coli* BL21 (DE3) cells transformed with overexpression constructs were grown in 2× YT medium containing 100 μg/ml ampicillin. Expression was induced with 1 mM isopropyl β-D-1-thiogalactopyranoside until OD_{600} reached 0.6. Protein purification was carried out at 4°C. The bacterial pellet was collected and lysed with 100 ml of lysis buffer (PBS, 500 mM NaCl [pH 7.4]). Cells resuspended in lysis buffer were broken by sonication on ice. After ultracentrifugation for 1 hr at 30,000 × *g* and 4°C, the supernatant was loaded onto a GST column (GE Healthcare). The target protein was cleaved on the column by PreScission Protease (GE Healthcare) overnight and then eluted in Superdex 75 buffer (25 mM Tris-HCl, 150 mM NaCl [pH 7.5]). After repeated gel filtration, pure holo-hDOHH was obtained.

For the preparation of ^{57}Fe-hDOHH, 20 mg of ^{57}Fe metal foil were dissolved in 18% HCl. After removal of HCl, $^{57}Fe^{3+}$ dissolved in water was added to 2 l of M9 minimal medium. The purification protocols were the same as for normal protein.

UV/Vis Spectra

A first measurement was carried out immediately after protein purification (following cleavage of the GST tag on the column) (at 4°C, 24 hr after breaking the cells). Around 5 mg/ml wild-type enzyme in Tris-HCl buffer (25 mM Tris-HCl, 150 mM NaCl [pH 7.5]) was used for time-dependent UV/Vis spectroscopic measurements. 1 ml of protein solution in a quartz cuvette was covered by a layer of paraffin oil. The sample was stored at 10°C and measured every 2 hr (during the first 12 hr) or every 12 hr (thereafter).

Mössbauer Spectra

^{57}Fe-labeled hDOHH in Tris-HCl buffer (see above) or in polycrystalline form was subjected to Mössbauer spectroscopy. Four different samples were measured: freshly isolated enzyme (prepared at 4°C), crystals grown from the fresh enzyme preparation (at 10°C, harvested 48 hr after setting up the crystallization experiment), enzyme in glycerol-containing buffer (stored at 10°C for 48 hr), and crystals grown in the presence of 10% glycerol (at 10°C, harvested 48 hr after setting up the crystallization experiment). Details of crystallization and Mössbauer spectroscopy experiments are presented in the Supplemental Experimental Procedures.

Crystallographic Studies

Optimized crystallization conditions were 30% polyethylene glycol 6000 (w/v), 400 mM guanidinium hydrochloride (Gdn·HCl), 100 mM Bis-Tris propane (pH 7.2–7.4). For the GLC complex, Gdn·HCl was replaced by 10%–20% glycerol. 48 hr after setting up the crystallization experiments, crystals were shock cooled and stored in liquid nitrogen. The structure of

GLC was determined using the single-wavelength anomalous diffraction (SAD) method with anomalous dispersion from the iron atoms; the structure of POX was solved by molecular replacement and GLC as the search model. Full details of crystallization, data collection, structure determination, refinement, and validation can be found in the Supplemental Experimental Procedures.

Automated Docking

Preparation of the target protein structure and the ligands was carried out by using AutoDock Tools (version 1.5.6) and docking was performed by AutoDock (version 4.2) (Morris et al., 2009). The crystal structure of hDOHH (POX) was used as the target protein. Iron ions were included in the docking grid with their charges set to +1. Iron ligands His56, His89, His207, and His240 were deprotonated. The grid box included the entire inner cavity and part of the external cavity. Structures of Dhp and Hpu were created using the *PRODRG* server (Schüttelkopf and van Aalten, 2004).

ACCESSION NUMBERS

The PDB accession number for the atom coordinates and structure factors of the crystal structures reported in this paper are 4D50 (POX structure) and 4D4Z (GLC structure).

SUPPLEMENTAL INFORMATION

Supplemental Information includes Supplemental Experimental Procedures, four figures, and two tables and can be found with this article online at http://dx.doi.org/10.1016/j.str.2015.03.002.

AUTHOR CONTRIBUTIONS

Z.H. made the overexpression construct, purified and crystallized hDOHH and its ^{57}Fe variant, collected diffraction data, solved and refined the structure, recorded the UV/Vis spectra, performed the mutagenesis experiments, and wrote the manuscript. N.S. collected the diffraction data and helped to solve the GLC structure. L.H.B. recorded and analyzed the Mössbauer spectra. S.K. purified the protein and performed early crystallization experiments. J.H. initiated the project and helped to write the manuscript. A.X.T. interpreted the Mössbauer spectra and wrote the manuscript. R.H. designed the experiments, interpreted the electron density maps, and wrote the manuscript.

ACKNOWLEDGMENTS

Access to beamline BL14.2 at the BESSY II electron storage ring (Helmholtz-Zentrum Berlin, Berlin-Adlershof, Germany) is gratefully acknowledged. This project was supported by the German Federal Ministry of Education and Research (BMBF; grant no. 01GUO718). R.H. thanks the DFG Cluster of Excellence "Inflammation at Interfaces" (EXC 206) for support.

Received: February 2, 2015
Revised: March 9, 2015
Accepted: March 10, 2015
Published: April 9, 2015

REFERENCES

Abbruzzese, A., Hanauske-Abel, H.M., Park, M.H., Henke, S., and Folk, J.E. (1991). The active site of deoxyhypusyl hydroxylase: use of catecholpeptides and their component chelator and peptide moieties as molecular probes. Biochim. Biophys. Acta *1077*, 159–166.

Bailey, L.J., and Fox, B.G. (2009). Crystallographic and catalytic studies of the peroxide-shunt reaction in a diiron hydroxylase. Biochemistry *48*, 8932–8939.

Bochevarov, A.D., Li, J., Song, W.J., Friesner, R.A., and Lippard, S.J. (2011). Insights into the different dioxygen activation pathways of methane and toluene monooxygenase hydroxylases. J. Am. Chem. Soc. *133*, 7384–7397.

Bou-Abdallah, F., Zhao, G., Mayne, H.R., Arosio, P., and Chasteen, N.D. (2005). Origin of the unusual kinetics of iron deposition in human H-chain ferritin. J. Am. Chem. Soc. *127*, 3885–3893.

Broadwater, J.A., Ai, J., Loehr, T.M., Sanders-Loehr, J., and Fox, B.G. (1998). Peroxodiferric intermediate of stearoyl-acyl carrier protein Δ^9 desaturase: oxidase reactivity during single turnover and implications for the mechanism of desaturation. Biochemistry *37*, 14664–14671.

Cano, V.S., Medrano, F.J., Park, M.H., and Valentini, S.R. (2010). Evidence for conformational changes in the yeast deoxyhypusine hydroxylase Lia1 upon iron displacement from its active site. Amino Acids *38*, 479–490.

Caraglia, M., Marra, M., Giuberti, G., D'Alessandro, A.M., Budillon, A., del Prete, S., Lentini, A., Beninati, S., and Abbruzzese, A. (2001). The role of eukaryotic initiation factor 5A in the control of cell proliferation and apoptosis. Amino Acids *20*, 91–104.

Caraglia, M., Park, M.H., Wolff, E.C., Marra, M., and Abbruzzese, A. (2013). eIF5A isoforms and cancer: two brothers for two functions? Amino Acids *44*, 103–109.

Dong, Y., Yan, S., Young, V.G., Jr., and Que, L., Jr. (1996). Crystal structure analysis of a synthetic non-heme diiron-O_2 adduct: insight into the mechanism of oxygen activation. Angew. Chem. Int. Ed. Engl. *35*, 618–620.

Facchiano, A.M., Stiuso, P., Chiusano, M.L., Caraglia, M., Giuberti, G., Marra, M., Abbruzzese, A., and Colonna, G. (2001). Homology modelling of the human eukaryotic initiation factor 5A (eIF-5A). Prot. Eng. *14*, 881–890.

Friedle, S., Reisner, E., and Lippard, S.J. (2010). Current challenges of modeling diiron enzyme active sites for dioxygen activation by biomimetic synthetic complexes. Chem. Soc. Rev. *39*, 2768–2779.

Frisch, J.R., Vu, V.V., Martinho, M., Münck, E., and Que, L., Jr. (2009). Characterization of two distinct adducts in the reaction of a nonheme diiron(II) complex with O_2. Inorg. Chem. *48*, 8325–8336.

Greganova, E., Altmann, M., and Bütikofer, P. (2011). Unique modifications of translation elongation factors. FEBS J. *278*, 2613–2624.

Gutierrez, E., Shin, B.S., Woolstenhulme, C.J., Kim, J.R., Saini, P., Buskirk, A.R., and Dever, T.E. (2013). eIF5A promotes translation of polyproline motifs. Mol. Cell *51*, 35–45.

Hanauske-Abel, H.M., Park, M.H., Hanauske, A.R., Popowicz, A.M., Lalande, M., and Folk, J.E. (1994). Inhibition of the G1-S transition of the cell cycle by inhibitors of deoxyhypusine hydroxylation. Biochim. Biophys. Acta *1221*, 115–124.

Hauber, I., Bevec, D., Heukeshoven, J., Krätzer, F., Horn, F., Choidas, A., Harrer, T., and Hauber, J. (2005). Identification of cellular deoxyhypusine synthase as a novel target for antiretroviral therapy. J. Clin. Invest. *115*, 76–85.

Holmes, M.A., Trong, I.L., Turley, S., Sieker, L.C., and Stenkamp, R.E. (1991). Structures of deoxy and oxy hemerythrin at 2.0 Å resolution. J. Mol. Biol. *218*, 583–593.

Kaiser, A. (2012). Translational control of eIF5A in various diseases. Amino Acids *42*, 679–684.

Kang, K.R., Kim, Y.S., Wolff, E.C., and Park, M.H. (2007). Specificity of the deoxyhypusine hydroxylase-eukaryotic translation initiation factor (eIF5A) interaction. J. Biol. Chem. *282*, 8300–8308.

Kim, K., and Lippard, S.J. (1996). Structure and Mössbauer spectrum of a (μ-1,2-peroxo)bis(μ-carboxylato)diiron(III) model for the peroxo intermediate in the methane monooxygenase hydroxylase reaction cycle. J. Am. Chem. Soc. *118*, 4914–4915.

Kim, Y.S., Kang, K.R., Wolff, E.C., Bell, J.K., McPhie, P., and Park, M.H. (2006). Deoxyhypusine hydroxylase is an Fe(II)-dependent, HEAT-repeat enzyme. Identification of amino acid residues critical for Fe(II) binding and catalysis. J. Biol. Chem. *281*, 13217–13225.

Klotz, I.M., and Kurtz, D.M., Jr. (1984). Binuclear oxygen carriers: hemerythrin. Acc. Chem. Res. *17*, 16–22.

Korboukh, V.K., Li, N., Barr, E.W., Bollinger, J.M., Jr., and Krebs, C. (2009). A long-lived, substrate-hydroxylating peroxodiiron(III/III) intermediate in the amine oxygenase, AurF, from *Streptomyces thioluteus*. J. Am. Chem. Soc. *131*, 13608–13609.

Kurtz, D.M., Jr. (1990). Oxo- and hydroxo-bridged diiron complexes: a chemical perspective on a biological unit. Chem. Rev. *90*, 585–606.

Lee, S.K., and Lipscomb, J.D. (1999). Oxygen activation catalyzed by methane monooxygenase hydroxylase component: proton delivery during the O-O bond cleavage steps. Biochemistry *38*, 4423–4432.

Lee, S.J., McCormick, M.S., Lippard, S.J., and Cho, U.S. (2013). Control of substrate access to the active site in methane monooxygenase. Nature *494*, 380–384.

Liu, K.E., Valentine, A.M., Qiu, D., Edmondson, D.E., Appelman, E.H., Spiro, T.G., and Lippard, S.J. (1995). Characterization of a diiron(III) peroxide intermediate in the reaction cycle of methane monooxygenase hydroxylase from *Methylococcus capsulatus* (Bath). J. Am. Chem. Soc. *117*, 4997–4998.

Maier, B., Ogihara, T., Trace, A.P., Tersey, S.A., Robbins, R.D., Chakrabarti, S.K., Nunemaker, C.S., Stull, N.D., Taylor, C.A., Thompson, J.E., et al. (2010). The unique hypusine modification of eIF5A promotes islet β cell inflammation and dysfunction in mice. J. Clin. Invest. *120*, 2156–2170.

McCormick, M.S., and Lippard, S.J. (2011). Analysis of substrate access to active sites in bacterial multicomponent monooxygenase hydroxylases: X-ray crystal structure of xenon-pressurized phenol hydroxylase from *Pseudomonas sp*. OX1. Biochemistry *50*, 11058–11069.

Moënne-Loccoz, P., Baldwin, J., Ley, B.A., Loehr, T.M., and Bollinger, J.M., Jr. (1998). O_2 activation by non-heme diiron proteins: identification of a symmetric μ-1,2-peroxide in a mutant of ribonucleotide reductase. Biochemistry *37*, 14659–14663.

Moënne-Loccoz, P., Krebs, C., Herlihy, K., Edmondson, D.E., Theil, E.C., Huynh, B.H., and Loehr, T.M. (1999). The ferroxidase reaction of ferritin reveals a diferric μ-1,2 bridging peroxide intermediate in common with other O_2-activating non-heme diiron proteins. Biochemistry *38*, 5290–5295.

Morris, G.M., Huey, R., Lindstrom, W., Sanner, M.F., Belew, R.K., Goodsell, D.S., and Olson, A.J. (2009). Autodock4 and AutoDockTools4: automated docking with selective receptor flexibility. J. Comput. Chem. *30*, 2785–2791.

Murray, L.J., Naik, S.G., Ortillo, D.O., García-Serres, R., Lee, J.K., Huynh, B.H., and Lippard, S.J. (2007). Characterization of the arene-oxidizing intermediate in ToMOH as a diiron(III) species. J. Am. Chem. Soc. *129*, 14500–14510.

Nordlund, P., and Eklund, H. (1995). Di-iron-carboxylate proteins. Curr. Opin. Struct. Biol. *5*, 758–766.

Ookubo, T., Sugimoto, H., Nagayama, T., Masuda, H., Sato, T., Tanaka, K., Maeda, Y., Ōkawa, H., Hayashi, Y., Uehara, A., et al. (1996). *cis*-μ-1,2-peroxo diiron complex: structure and reversible oxygenation. J. Am. Chem. Soc. *118*, 701–702.

Pandelia, M.E., Li, N., Nørgaard, H., Warui, D.M., Rajakovich, L.J., Chang, W.C., Booker, S.J., Krebs, C., and Bollinger, J.M., Jr. (2013). Substrate-triggered addition of dioxygen to the diferrous cofactor of aldehyde-deformylating oxygenase to form a diferric-peroxide intermediate. J. Am. Chem. Soc. *135*, 15801–15812.

Park, M.H. (2006). The post-translational synthesis of a polyamine-derived amino acid, hypusine, in the eukaryotic translation initiation factor 5A (eIF5A). J. Biochem. *139*, 161–169.

Park, J.H., Aravind, L., Wolff, E.C., Kaevel, J., Kim, Y.S., and Park, M.H. (2006). Molecular cloning, expression, and structural prediction of deoxyhypusine hydroxylase: a HEAT-repeat-containing metalloenzyme. Proc. Natl. Acad. Sci. USA *103*, 51–56.

Saini, P., Eyler, D.E., Green, R., and Dever, T.E. (2009). Hypusine-containing protein eIF5A promotes translation elongation. Nature *459*, 118–121.

Schüttelkopf, A.W., and van Aalten, D.M. (2004). *PRODRG*: a tool for high-throughput crystallography of protein-ligand complexes. Acta Crystallogr. D Biol. Crystallogr. *60*, 1355–1363.

Solomon, E.I., Brunold, T.C., Davis, M.I., Kemsley, J.N., Lee, S.K., Lehnert, N., Neese, F., Skulan, A.J., Yang, Y.S., and Zhou, J. (2000). Geometric and electronic structure/function correlations in non-heme iron enzymes. Chem. Rev. *100*, 235–350.

Song, W.J., and Lippard, S.J. (2011). Mechanistic studies of reactions of peroxodiiron(III) intermediates in T201 variants of toluene/*o*-xylene monooxygenase hydroxylase. Biochemistry *50*, 5391–5399.

Song, W.J., Behan, R.K., Naik, S.G., Huynh, B.H., and Lippard, S.J. (2009). Characterization of a peroxodiiron(III) intermediate in the T201S variant of toluene/*o*-xylene monooxygenase hydroxylase from *Pseudomonas* sp. OX1. J. Am. Chem. Soc. *131*, 6074–6075.

Song, W.J., McCormick, M.S., Behan, R.K., Sazinsky, M.H., Jiang, W., Lin, J., Krebs, C., and Lippard, S.J. (2010). Active site threonine facilitates proton transfer during dioxygen activation at the diiron center of toluene/*o*-xylene monooxygenase hydroxylase. J. Am. Chem. Soc. *132*, 13582–13585.

Stenkamp, R.E. (1994). Dioxygen and hemerythrin. Chem. Rev. *94*, 715–726.

Summa, C.M., Lombardi, A., Lewis, M., and DeGrado, W.F. (1999). Tertiary templates for the design of diiron proteins. Curr. Opin. Struct. Biol. *9*, 500–508.

Tome, M.E., and Gerner, E.W. (1997). Cellular eukaryotic initiation factor 5A content as a mediator of polyamine effects on growth and apoptosis. Neurosignals *6*, 150–156.

Vu, V.V., Emerson, J.P., Martinho, M., Kim, Y.S., Münck, E., Park, M.H., and Que, L., Jr. (2009). Human deoxyhypusine hydroxylase, an enzyme involved in regulating cell growth, activates O_2 with a nonheme diiron center. Proc. Natl. Acad. Sci. USA *106*, 14814–14819.

Wallar, B.J., and Lipscomb, J.D. (1996). Dioxygen activation by enzymes containing binuclear non-heme iron clusters. Chem. Rev. *96*, 2625–2658.

Weiss, M.S., and Hilgenfeld, R. (1997). On the use of the merging *R* factor as a quality indicator for X-ray data. J. Appl. Cryst. *30*, 203–205.

Xue, G., Fiedlera, A.T., Martinho, M., Münck, E., and Que, L., Jr. (2008). Insights into the P-to-Q conversion in the catalytic cycle of methane monooxygenase from a synthetic model system. Proc. Natl. Acad. Sci. USA *105*, 20615–20620.

Zhang, X., Furutachi, H., Fujinami, S., Nagatomo, S., Maeda, Y., Watanabe, Y., Kitagawa, T., and Suzuki, M. (2005). Structural and spectroscopic characterization of (μ-hydroxo or μ-oxo)(μ-peroxo) diiron(III) complexes: models for peroxo intermediates of non-heme diiron proteins. J. Am. Chem. Soc. *127*, 826–827.

